Benajes, J.; Novella Rosa, R.; Gómez-Soriano, J.; Barbery-Avila, II.; Libert, C.; Rampanarivo, F.; Dabiri, M. (2020). Computational assessment towards understanding the energy conversion and combustion process of lean mixtures in passive pre-chamber ignited engines. Applied Thermal Engineering. 178:1-17. https://doi.org/10.1016/j.applthermaleng.2020.115501

Computational assessment towards understanding the energy conversion and combustion process of lean mixtures in passive pre-chamber ignited engines

J. Benajes[a], R. Novella[a,*], J. Gomez-Soriano[a], I. Barbery[a], C. Libert[b], F. Rampanarivo[b], M. Dabiri[b]

[a]*CMT – Motores Térmicos, Universitat Politècnica de València, Camino de Vera, 46022 Valencia, Spain*
[b]*DEA-IRP Groupe Renault, 1 avenue du Golf. 78084, Guyancourt, France*

Abstract

The passive pre-chamber ignition concept is becoming a popular technology for engine applications as packaging and installation is very simple and straightforward. The implementation of this ignition strategy becomes even more attractive in combination with lean combustion, as the combustion process occurs much faster, improving the thermal efficiency of the engine. However, not much effort has been made to study this concept as it has considerable disadvantages when compared with the active system. In this framework, a computational study was performed using a combination of several numerical tools to better understand the limiting aspects of combustion in the passive pre-chamber ignition system when operating at lean conditions. A specific methodology was developed to analyse in detail the scavenging and combustion processes of this ignition concept. Results show how the scavenging of passive pre-chambers is primarily dependent on the force that the piston makes on the gas during the compression stroke, being independent of the pre-chamber geometry as along as the ratio between the total cross sectional area of the pre-chamber holes and the pre-chamber volume is kept within a suitable range. Moreover, a successful lean combustion cannot be achieved as the burning rates inside the pre-chamber significantly decrease due to the low laminar flame speeds, that results in low quality ejected jets. Further results show that increasing the flow temperature can help to recover competitive combustion rates when knocking combustion is not a limiting factor. Alternatives for increasing the laminar flame speed were proposed in order to improve combustion inside the pre-chamber. Although the pre-chamber combustion profile was successfully improved, none of the proposed solutions were able to completely burn the main chamber charge with the current pre-chamber design.

Keywords: *spark-ignition engines, passive pre-chamber, ultra-lean combustion, pre-chamber scavenge, CFD combustion modelling, energy conversion*

1. Introduction

Nowadays regulations for air polluting emissions are becoming more and more restrictive, and particularly for the transportation sector fulfilling these regulations while maintaining or even improving the engine efficiency is of great interest. According to the International Energy Outlook journal's review [1], the transportation vehicles share of worldwide energy consumption is approximately 28%, increasing at an annual rate of 1.4%. These vehicles are also responsible for a high percentage of carbon monoxide (CO) and nitrous oxides (NO_x) emissions [2]. Based on recent trends, spark-ignition (SI) engines are becoming the main powerplant in the passenger car market, displacing compression-ignition (CI) engines. Although the main reason for this replacement is the restrictive environmental problem [3], it is known that SI engines provide worse efficiency than equivalent CI engines due to their low compression ratios and the necessity of operating them at stoichiometric conditions for compatibility with the state of the art 3-way catalyst [4, 5]. This fact motivates the study of different alternatives to improve engine efficiency and fuel consumption while maintaining the low pollutant emissions in SI engines.

In a first approach, increasing the engine compression ratio (that typically ranges from 8:1 to 12:1) to match those commonly used in CI engines (14:1–16:1) seems to be a straightforward solution to improve the thermal efficiency of the engine [6, 7]. However, knocking combustion [8] becomes the main limiting factor for gasoline fuel [9] due to the increased heat transfer [10, 11] and engine integrity issues [12, 13]. Many authors have investigated other strategies for achieving higher efficiency. For example, the well-known Miller cycle [14, 15] that reduces the pumping losses to near-zero values at part loads. However, this strategy usually deteriorates the turbulence properties in the cylinder, compromising the combustion process when closing the intake valve at earlier stages. Also, it is worth to mention alternative combustion processes that will be mainly based on charge stratification or new fuels [16].

Probably the most promising of these strategies is the operation with lean mixtures. Burning lean air-fuel mixtures has shown the capability to improve the engine efficiency in

*Corresponding author.
Tel.: +34 96 387 98 13, fax: +34 96 387 76 59
email: rinoro@mot.upv.es

several ways. First, the heat losses through the combustion chamber walls are significantly reduced as the combustion temperatures reached during the closed cycle are lower [17]. Moreover, lean operation can also reduce the pumping losses of the engine at medium-to-low loads. Conventional SI engines operating at partial loads use a throttle valve to restrict the intake flow, which contributes significantly to the engine pumping work [18, 19]. However, if the engine can successfully operate with lean mixtures, the load can be controlled directly through the amount of fuel injected during the cycle. In this way, and depending on the required load and lean operating limit, the engine may be able to operate at wide open throttle or at least with only partial throttling. Moreover, the specific heat ratio (γ) of the air-fuel mixture increases with an increase of the relative air-to-fuel ratio (λ). In this case the thermal efficiency of the engine, which depends only on the compression ratio and the γ of the fluid for an ideal Otto cycle [20], is improved through the increment of γ.

Nonetheless, there are several drawbacks associated with operating SI engines with lean mixtures. The speed at which flame propagates is decreased as λ increases, leading to longer burning times, incomplete combustion and high cycle-to-cycle variations that are detrimental to the engine performance. Besides, the ignition of lean mixtures becomes more complicated as the amount of air increases [21].

In order to overcome these issues, several ignition and combustion strategies such as Gasoline Compression Ignition (GCI) [22, 23], stratified charge combustion using Gasoline Direct Injection (GDI) [24] and pre-chamber ignition [25, 26] have been widely investigated. In particular, the pre-chamber ignition concept, being widely established in high power stationary powerplants [27], arises as a very promising solution for future SI engines. This concept, also known as Turbulent Jet Ignition (TJI) in the frame of automotive applications, is currently being the focus of many research efforts [28, 29].

However, physical phenomena involved in the pre-chamber ignition concept are still not clearly understood. From the point of view of combustion, numerous research works [25, 30, 31] have shed some light on the interaction between combustion and turbulence. In particular, they identified some of the key aspects of the concept by determining the flame regime under TJI combustion. Nevertheless, the effect of energy conversion within the pre-chamber on the performance and efficiency of the concept has not been evaluated yet. In that sense, heat transfer and energy losses due to ejection of cold/non-reacting mixture could play a significant role on the concept performance.

2. Pre-chamber ignition concept

The TJI concept is an ignition strategy that uses a standard spark plug to initiate combustion and two combustion chambers connected to each other by one or more small holes [32, 30]. Typically, these holes are simple cylinders. The larger of the chambers is the conventional SI combustion chamber, while the smaller one, having a fixed volume, is where combustion is initiated by the spark plug. The latter, known as the "pre-chamber", usually occupies a volume that is roughly between 2% and 5% of the cylinder volume at Top Dead Center (TDC) in Internal Combustion Engine (ICE) applications [33, 19]. As the flame propagates in the pre-chamber, the mean pressure rises forcing the gas to move towards the main chamber. As a result of the stretching though the small orifices, high turbulent jets penetrate into the main chamber, igniting the charge with higher surface contact at multiple locations. The generation of turbulence produced by the shear of the jet flow increases flame propagation speeds. Moreover, the jets distribute hot gases and combustion products over a wide region in the main chamber generating dispersed and uniform ignition throughout the sweped volume. In view of these, several authors [34, 35] have demonstrated how the TJI concept is well suited to mitigate the negative effects of the low flame speeds associated to lean combustion in conventional SI engines.

The pre-chamber ignition concept can be implemented according to two approaches, active and passive systems [36]. In active systems there is an auxiliary fuel supplier inside the pre-chamber, thereby its air-to-fuel ratio is controlled at optimum values close to stoichiometric conditions, independently from that of the main chamber, which usually operates with λ values between 2.0 and 2.5 for gasoline fuel [31, 37]. Such elevated air-to-fuel ratios reduce combustion temperatures well below 1800K, consequently reducing NO_x emissions to near-zero values since the activation energy for nitrogen oxidation through the Zeldovich thermal mechanism is not reached [38].

In passive systems there is no auxiliary fuel supplied into the pre-chamber, thus its air-to-fuel ratio is not directly controlled [39]. In Port Fuel Injection (PFI) engines the main chamber and the pre-chamber λ is essentially the same, causing the ignition and propagation issues found in conventional SI operation to be transferred to the pre-chamber. On the other hand, for GDI engines the difference between both chambers in λ can be indirectly controlled, at least up to some extent [40], by the relative position among the injector and the pre-chamber. Although this concept has considerable disadvantages in comparison with the active system, it is very attractive for passenger car applications since packaging and installation is very simple and straightforward. However, the understanding of the physical limitations of this particular concept is still very limited, especially those aspects related to the pre-chamber scavenge and the ignition limits when extending the λ range to values where NO_x formation is avoided [41].

The main purpose of this paper is therefore to improve knowledge of the passive pre-chamber ignition system. Particularly, the analysis and understanding of the pre-chamber scavenge and misfiring events when operating at ultra-lean conditions ($\lambda \geq 2$) are addressed. Moreover, the energy conversion inside the pre-chamber has been analysed in detail in order to show whether the energy losses associated with HT and gas ejection phenomena have a relevant impact on the concept itself. Several numerical tools, including 0D, 1D and

3D Computational Fluid Dynamics (CFD), were used to provide additional insight on these questions, overcoming the limitations of experiments.

3. Tools and methodology

A computational study combined with a set of measurements was performed to understand the passive pre-chamber ignition concept in a turbocharged single-cylinder PFI SI engine. Several numerical tools (0D, 1D and CFD models), previously validated with experimental tests, were combined to better understand the characteristics and limitations of this ignition concept.

3.1. Experimental set-up

Experimental activities were carried out in a single-cylinder research version of a 4-stroke turbocharged SI engine, which due to its high compression ratio and low cylinder displacement, is a perfect sample of near future engines to be used in passenger car applications. The engine is equipped with a PFI system assembled in the intake manifold, 270 mm away from the cylinder head, to assure a complete mixing process between the air and the fuel. The cylinder head had four valves with double-overhead camshafts to improve the cylinder filling and scavenge. The small housing for the conventional spark plug is also used for the passive pre-chamber, to enable an easy exchange between these two ignition systems. The most relevant characteristics of the engine are shown in Table 1 for reference.

Table 1: *Main specifications of the engine.*

Engine	**4-stroke SI**
Number of cylinders [-]	1
Displacement [cm^3]	404
Bore – Stroke [mm]	80.0 – 80.5
Compression ratio (geometric) [-]	13.4:1
Valvetrain [-]	DOHC
Number of valves/cylinder [-]	2 intake and 2 exhaust
Fuel injection system [-]	PFI (p_{max} = 6 bar)

The engine was assembled into a fully instrumented test cell that included: an external compressor for providing air to simulate boost conditions, a low pressure EGR system designed to provide arbitrary levels of cooled EGR even at very high intake boost pressures, and different devices to control and measure parameters such as the water, oil and fuel temperatures, fuel consumption, pollutant emissions and in-cylinder air-to-fuel ratio. A piezoelectric sensor was placed inside the combustion chamber to measure instantaneous in-cylinder pressure with a resolution of 0.2 CAD.

The experiments were carried out at medium-load and medium-speed conditions shown in Table 2 as these gather intermediate points in the engine map, appropriate for the concepts characterization as high-load and low-load limitations are not considered [42]. A calibrated gasoline with the 95 Research Octane Number (RON) fuel was used for the tests.

Table 2: *Experimental baseline test conditions.*

PC ignition baseline	
Engine speed [rpm]	2000
IMEP [bar]	6.8
Injected fuel [mg/cc]	15.3
Intake air temperature [K]	302
Intake pressure [bar]	0.68
Exhaust pressure [bar]	1.04
coolant and oil temperature [K]	360

3.2. Numerical tools

3.2.1. Combustion diagnosis

A zero-dimensional combustion diagnosis tool was used to calculate the average cycle values of combustion related parameters from the measured in-cylinder pressure signal [43, 44]. The heat release due to combustion was included for a deeper analysis of the combustion process. In the case of experiments, this parameter was obtained by solving the energy equation with the in-cylinder pressure measurement and assuming several simplifications [45]. The equation is solved assuming uniform pressure and temperature fields through the whole combustion chamber and it yields the instantaneous mean temperature and the heat release. The latter parameter can be obtained considering additional hypotheses that allow to separate heat transfer losses towards the walls and the apparent Heat Release Rate (HRR). Other parameters obtained with this tool were the indicated gross mean effective pressure (IMEP), the combustion phasing (CA50), and the combustion duration (CA1090).

3.2.2. CFD model

The CFD simulations presented in this study were carried out using the CONVERGE v2.4 CFD software [46], a commercial code based on the finite volume method and developed primarily for ICE simulations.

The in-cylinder turbulence was modelled in an unsteady Reynolds-averaged Navier–Stokes (URANS) framework by using a well-known eddy-viscosity-based two-equation turbulence model, namely the Re-Normalization Group variant of the k-epsilon model (RNG k-ϵ model), widely extended in ICE applications [47, 48]. The wall heat-transfer model developed by Angelberger [49] was used to account for heat losses through the boundaries of the computational domain. The Redlich-Kwong equation [50] was selected as the equation of state for calculating the compressible flow properties.

For combustion modeling a two-zone flame front tracking model, more specifically the extended coherent flamelet model (ECFM) was chosen [51, 52]. This model tracks the flame propagation by solving a transport equation for the flame surface density (Σ) that in addition to the classical unsteady convection and diffusion terms, also accounts for the turbulent stretch, thermal expansion and mean flow dilation of the flame [53, 54]. The resulting flame front is used to describe large scale burned/unburned stratification for the species. Although the model does not account for detailed

chemistry, it can accurately describe the propagation of turbulent premixed flames [55], making it suitable for predicting the combustion process in SI engines. Simultaneously, the computational time associated to this model is considerably lower when compared to detailed chemistry calculations, as the transport equations for species are extensively reduced.

As detailed chemistry is not solved, the ECFM model requires a Tabulated Kinetic Ignition (TKI) table to account for end-gas auto-ignition combustion. This model uses the auto-ignition delay values for the air-fuel blend in a wide range of pressure, temperature, equivalence ratio and composition. Similarly, an additional table with the laminar flamespeeds of the mixture is needed. These two tables where calculated previous to the simulation with the utilities available in the software.

The model is coupled with an imposed stretch spark ignition model (ISSIM) which simulates the spark discharge and breakdown. This is based on resolving the ordinary differential equation for a simplification of the spark plug electrical circuit [56, 57], which starts from a setting energy input and ultimately deposits an initial flame kernel in form of a sphere and with a reference flame surface density for the transport equation.

For the numerical solver a second-order central difference scheme has been used for spatial discretization, a first-order scheme for temporal discretization and a modified Pressure Implicit with Splitting of Operators (PISO) algorithm was chosen to couple the momentum, energy and the other transport equations [58].

Fig. 1 shows the computational domain created from the real engine geometry, including the intake/exhaust ports and the pre-chamber. As can be seen the pre-chamber is not aligned with respect to the cylinder axis due to the particular design of the cylinder head. Hexahedral meshing was used for the whole computational domain with a base cell size of 4 mm. The mesh in the intake and exhaust conducts was refined to 2 mm, while a 1 mm refinement was applied inside the cylinder. The cell size near the cylinder walls, including the moving piston and valves, was reduced down to 0.5 mm to improve boundary layer prediction. In the pre-chamber region, the cell size was fixed to 0.25 mm and 0.125 mm for cells located close to the walls. Moreover, Adaptive Mesh Refinement (AMR) was used to improve grid resolution. This algorithm increases the grid resolution based on velocity and temperature sub-grid criteria of 1 m/s and 2.5 K up to a minimum cell size of 0.125 mm. Finally, the mesh was refined to 0.0625 mm at the spark gap location to better capture the initial flame kernel and the early combustion evolution.

Regarding the boundary conditions, wall temperatures for the piston, liner and cylinder head were estimated from the experiments by the lumped model proposed by Torregrosa et al. [59]. Instantaneous pressure and temperature measurements at the intake/exhaust manifolds were used as inflow/outflow boundary conditions.

3.2.3. Auto-ignition delay calculations

As explained in the previous section, the ECFM combustion model requires tabulated values of the auto-ignition delay to predict knocking combustion of the air/fuel mixture. For this purpose a set of zero-dimensional calculations were performed using a OD homogeneous reactor model, assuming constant pressure conditions. This tool generates ignition delay data for different combinations of temperature, pressure, equivalence ratio and composition. The computed ignition delay is defined as the time required for the temperature to increase 400K from its initial value.

A required input parameter for performing these calculations was a chemical kinetic mechanism for a suitable gasoline surrogate. In this case a Primary Reference Fuel (PRF) was selected. Different mechanisms from the literature [60, 61, 62, 63] were tested and validated against experimental data from Fieweger et al. and Davidson et al. [64, 65]. the validation is shown in Fig. 2 where the auto-ignition delays for the selected reaction mechanisms were compared in stoichiometric conditions at 4 MPa of pressure and ultra-lean conditions ($\lambda = 2$) at 5 MPa. Few differences were found between all considered mechanisms, therefore the mechanism from Liu et al. [60] was chosen for its good balance among computational requirements and accuracy.

3.2.4. Laminar flame speed calculations

The laminar flame speeds of the air/fuel mixture are also required by the ECFM combustion model. This flame speed is usually calculated by using empirical correlations such as Metghalchi and Keck's [66] or Gulder's [67] equations. However, these functions tend to under-predict the laminar flame speeds at real engine conditions. As an alternative to these correlations, the ECFM combustion model can read these laminar flame speeds from a user defined table, generated from a 1D model. This tool calculates the flame speed of the combustion reaction using a freely propagating flame in a channel with fixed cross-sectional area for a specified temperature, pressure, equivalence ratio and composition.

A chemical kinetic mechanism is also needed to perform these calculations. Again, several mechanisms available in the literature [60, 61, 68] were selected to check their consistence with the experiments performed by Jerzembeck et al. and Heimel et al. [69, 70]. Fig. 3 shows an example of this comparison when considering engine-like conditions. In addition, the calculation with Metghalchi and Keck's correlation is included for reference. The mechanism from Liu et al. [60] was again selected, as it evidently gives the most accurate predictions.

3.2.5. Validation of CFD simulations

Prior to start with the analysis of combustion, the validation of the CFD model is a first and required step to assure the validity of the numerical solution. For this purpose, the operating point described in Table 2 was considered. Therefore, the in-cylinder pressure and HRR were compared to those

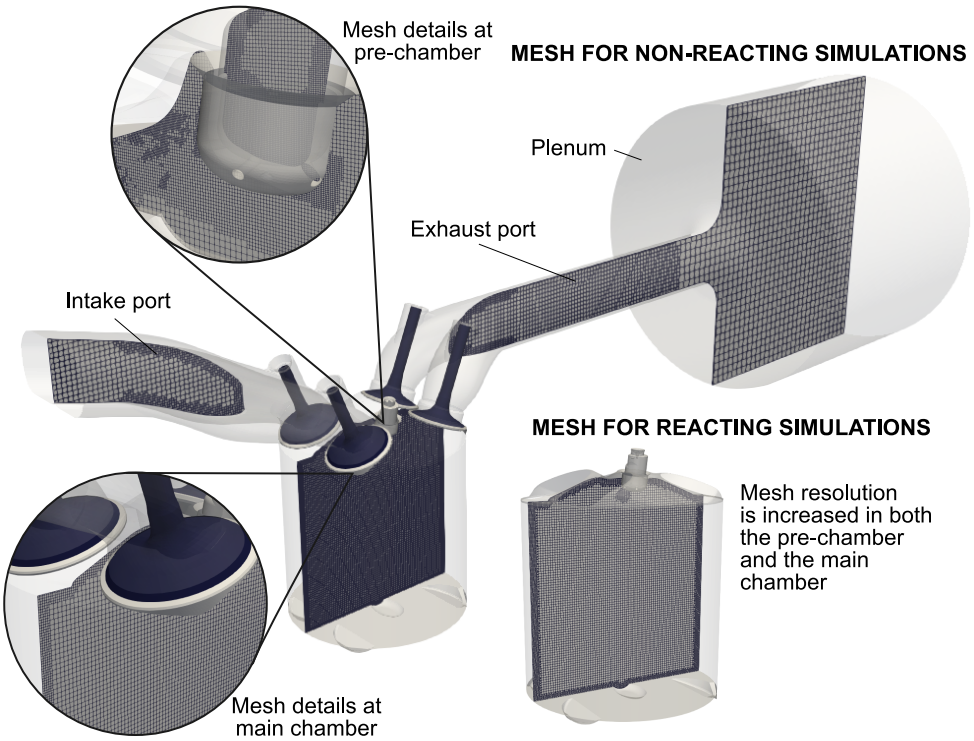

Figure 1: *Computational domain and mesh details for non-reacting and reacting simulations.*

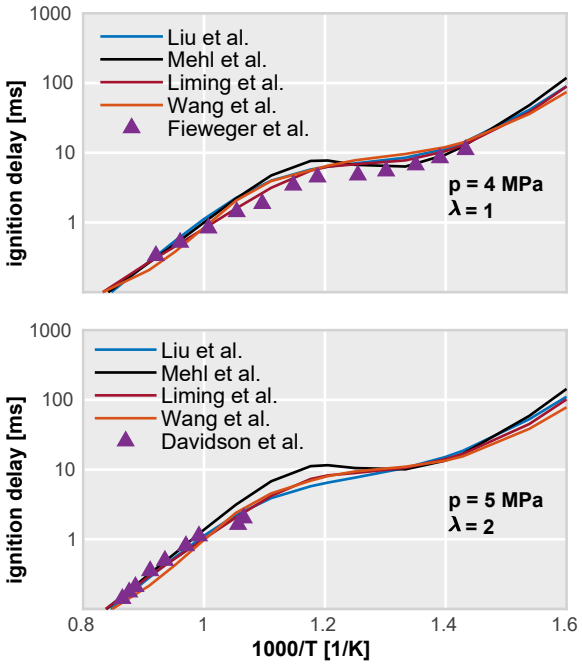

Figure 2: *Auto-ignition delays validation for different iso-octane mechanisms at engine-like conditions.*

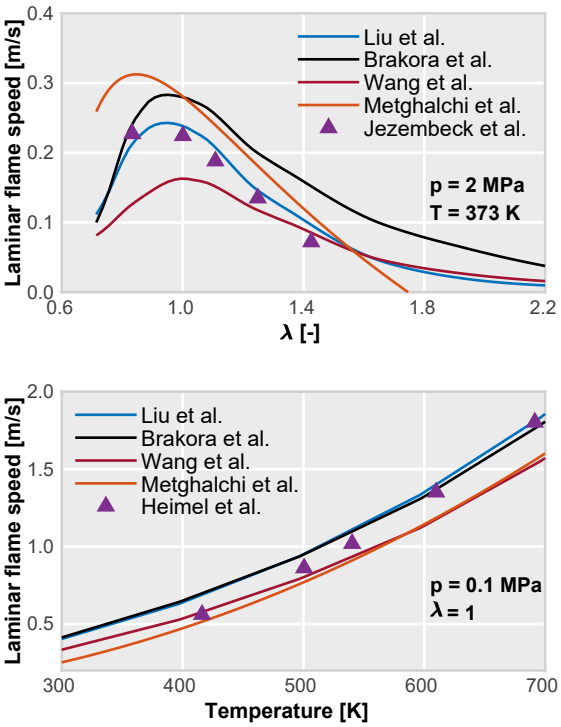

Figure 3: *Laminar flame speed validation for different iso-octane mechanisms at engine-like conditions.*

measured in the single cylinder engine considering both conventional spark and TJI concepts. Both tests were performed at stoichiometric conditions, and the conventional SI test was also included to reinforce the strength of the CFD model in a

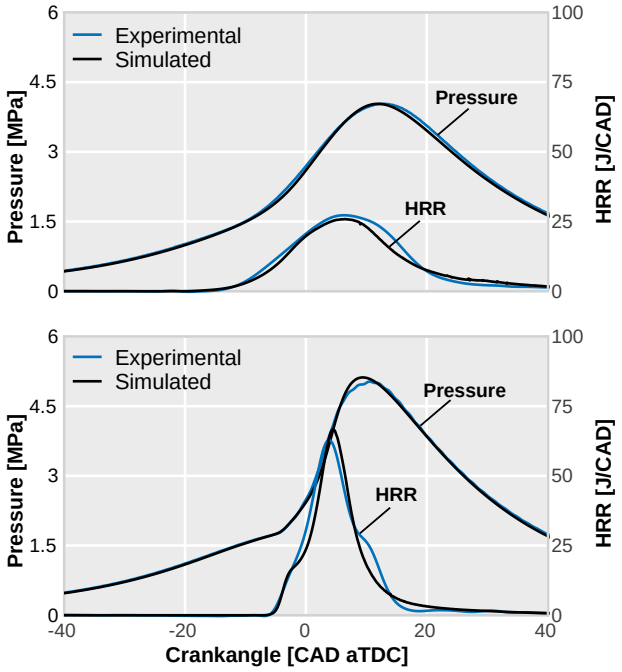

Figure 4: *Experimental validation of the CFD model in terms of in-cylinder pressure and rate of heat release operating with conventional SI (top) and TJI (bottom) concepts.*

well-validated and established combustion concept [71, 11]. In the TJI test, the pre-chamber design denoted as PC1 in Table 3 was used.

Results of this comparison are plotted in Fig. 4, in which the in-cylinder pressure data averaged over 250 measured cycles and the estimated HRR in the main chamber are included for both combustion concepts. It can be seen a good agreement among the simulation and experiment pressures thorough the closed-cycle. In addition, the HRR trace is also well captured by the numerical model, showing a good ignition onset and both maximum combustion rate and duration.

3.3. Methodology

Since there is limited literature related to modelling the pre-chamber ignition concept for automotive applications, a detailed methodology needs to be established in order to avoid possible numerical uncertainties and to assure a suitable analysis of the results. This methodology was divided into two main sections with several steps in between. First, the analysis of the pre-chamber filling (scavenge) was performed with non-reacting CFD simulations and secondly, the combustion process and energy conversion was deeply investigated by reacting simulations. Fig. 5 shows a summary of the work-flow followed in this research.

As the passive system has no auxiliary fuel injector, the evacuation of residual gases from the previous cycle, which are detrimental for the ignition and later flame propagation, becomes more intricate. Hence, a study of pre-chamber geometrical parameters was performed in order to determine how the combination of these parameters impacts the residual gases within the pre-chamber. However, since the level of complexity of the pre-chamber design can be very high, only some fundamental parameters were considered for this study: the pre-chamber volume, number of holes, hole diameter, and finally the ratio between the total cross-sectional area of the holes and the pre-chamber volume (A/V ratio).

Non-reacting CFD simulations were carried out for different pre-chamber designs, varying the aforementioned geometrical parameters. Each design was simulated during a complete engine cycle. Besides, in order to monitor the amount of fresh gases present in the pre-chamber, a set of tracers were defined for tracking the origin of the resulting flow inside the cylinder and the pre-chamber.

In the second section, the combustion process was analysed in the TJI configuration experimentally validated. The numerical solution was compared against in-cylinder pressure measurements and their estimated HRR profiles. Finally, additional combustion simulations were carried out at ultra-lean conditions ($\lambda = 2$) to analyse the limitations of the ignition concept when operating with high levels of air-dilution and to evaluate potential alternatives for extending the λ limit. Here, not only the most relevant parameters of combustion were analysed for both the pre-chamber and main chamber (HRR, Laminar flame speed, combustion regime), but also an energy balance inside the pre-chamber was performed to analyse the energy conversion during the ejection process. Therefore, the amount of energy lost by heat transfer and cold/non-reacting mixture ejection was estimated to determine the contribution of them to the overall performance of the concept, establishing the relationship between the energy available in the pre-chamber and the effective ignition of the main chamber.

All combustion simulations were executed in a reduced version of the original CFD domain as shown in the bottom-right side of Fig. 1. In this domain, the intake/exhaust ports and valves were removed to reduce the number of cells and the associated extra computational cost. Only the closed cycle was simulated in these cases, starting from a solution generated by the corresponding non-reacting simulation at the Intake Valve Closing (IVC) to conserve aerodynamics and species stratification, and ending at the Exhaust Valve Opening (EVO).

4. Results and discussion

This section discusses the results obtained after applying the described methodology, starting form the analysis of the scavenging process in the different pre-chamber designs considered for this study. Thereafter, the CFD combustion solution is compared and validated against the measurements at equivalent experimental conditions and pre-chamber design. Finally, the analysis of reacting simulations at ultra-lean conditions ($\lambda = 2$) is presented and the limitations of the TJI concept are investigated in detail.

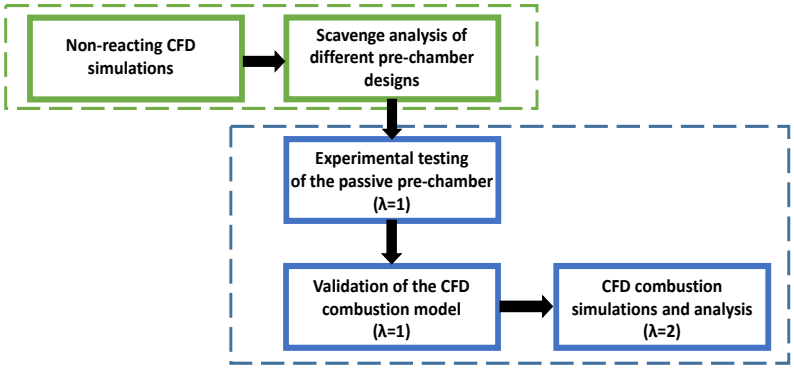

Figure 5: *Diagram of the methodology developed for the present research work.*

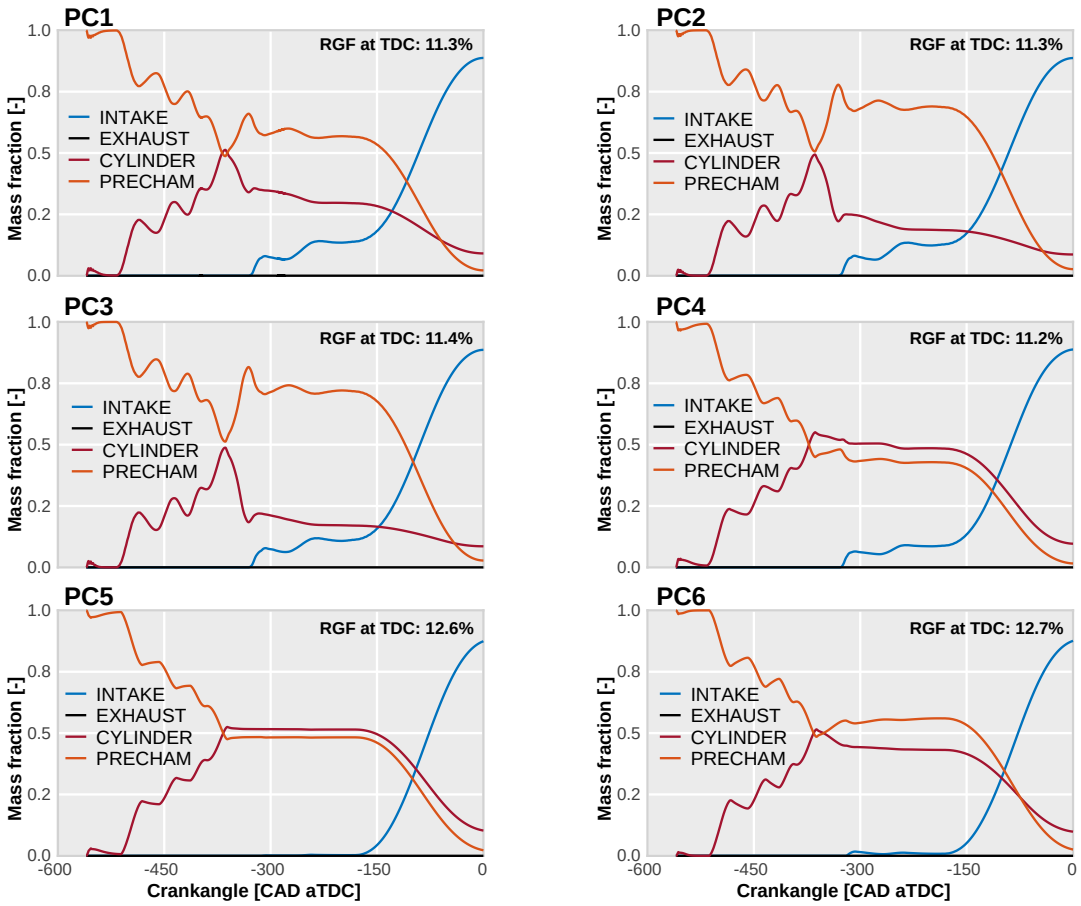

Figure 6: *Scavenge diagrams for the considered pre-chamber designs. The origin of the different flows are tracked by the defined tracers.*

4.1. Analysis of the pre-chamber scavenge

The non-reacting simulations were performed for the different pre-chamber designs shown in Table 3. The geometrical parameters considered for the pre-chamber configuration were the volume, number of holes and hole diameter. The ratio between the total cross-sectional area of the holes and the pre-chamber volume (A/V ratio) was also considered as a design parameter, as it directly relates the area available for the flow exchange with the volume to be filled. In this table, some of the parameters have been normalized by the reference design (PC1) values.

The analysis of the pre-chamber filling was performed through the scavenge diagrams included in Fig. 6. In these diagrams, the evolution of the pre-chamber filling is plotted from the EVO until the Top Dead Centre (TDC) of the com-

Table 3: *Pre-chamber designs and specifications.*

ID	Normalized volume [-]	Holes [-]	Normalized diameter [-]	A/V ratio [1/m]
PC 1	1.0	6	1.0	3.9
PC 2	1.6	6	1.3	3.9
PC 3	1.6	10	1.0	4.1
PC 4	0.6	4	1.0	4.4
PC 5	0.6	4	0.7	2.2
PC 6	1.6	6	0.7	1.2

pression stroke to observe the origin of the resultant flow within the pre-chamber. The Residual Gas Fraction (RGF) remaining inside the pre-chamber at TDC is included in the top right corner of each plot. As it can be seen, the mass exchange during the expansion/exhaust strokes ends with a mix of products remaining in the pre-chamber and coming from the cylinder. Those tracers represent the fraction of residual gases left in both chambers after combustion and the concentration of each one depends on the pre-chamber volume and A/V ratio. After the Intake Valve Opening (IVO) and during the intake stroke, part of the flow coming from the intake enters on the pre-chamber due to its proximity to the flow-path through the intake valves. By contrast, this particular behaviour is not observed in PC5 and PC6 due to the small diameter of the holes.

However, the contribution of the intake stroke to the overall filling of the pre-chamber is still very small (less than 15% of the pre-chamber is filled with fresh gases during this stroke). The effective pre-chamber filling takes place mainly during the compression stroke, when the piston forces the intake gases to enter the pre-chamber. This has some implications when advancing the spark timing (ST) since the RGF increases up to 16% with the ST triggered at -40 Crank Angle Degrees after Top Dead Centre (CAD aTDC). The scavenging of passive pre-chambers is thus mainly controlled by the compression ratio, being somehow independent of the pre-chamber geometry as long as a reasonable A/V ratio is considered. Large hole diameters may lead to a rapid loss of fuel mass towards the main chamber when the combustion starts in the pre-chamber, impeding to increase the pre-chamber pressure and therefore a suitable ejection [42]. On the contrary, very small orifices increase the pressure losses through the holes compromising the pre-chamber filling and scavenge (as it happens with PC6).

It is evident that despite the differences observed, there are no large changes in the effective RGF when considering a reasonable range of spark timing (among -40 and 0 CAD aTDC). Nonetheless, this value is slightly higher as the A/V ratio decreases. For instance, it is interesting to note that the minimum RGF (the values at TDC shown in Fig. 6) scarcely varies by 0.1% when the A/V ratio ranges from 3.9 to 4.4, whereas it increases by 1.5% (approx.) when decreasing the A/V ratio down to 1.2. Hence, as combining basic geometric parameters shows similar scavenging performance without taking into account the specific geometry, there is an interesting degree of freedom to optimize the concept by other relevant and more specific parameters such as the internal geometry and/or orientation of the holes, among others.

Lastly, examination of the scavenge diagrams reveals that there is a significant amount of residual gases that cannot be evacuated from the pre-chamber, contributing to decrease the laminar flame speed and ultimately reducing the tolerance of this ignition concept to external EGR dilution [42, 72].

4.2. Exploring the limits of ultra-lean combustion

Once the pre-chamber scavenge has been well-understood and after validating the CFD model in reacting conditions (see section 3.2.5), the model was used to gain insight about the flame propagation issues observed when operating at ultra-lean conditions [42]. In this case, a relative air-to-fuel ratio of 2 was considered since it prevents the (NO_x) formation by the Zeldovich thermal mechanism [38].

In Fig. 7, a comparison between stoichiometric ($\lambda = 1$) and ultra-lean ($\lambda = 2$) conditions for the TJI concept is shown. The evident pressure gap observed among both simulations during compression is caused by the fact that the target operating conditions were achieved by fixing the fuel quantity (the same amount as in the $\lambda = 1$ test) and increasing the intake pressure until the desired relative air-to-fuel ratio was reached. As expected from previous investigations, the HRR in the lean case is very low due to the flame propagation issues in both pre-chamber and main chamber. The low flame propagation speeds lead to extremely low combustion efficiency levels (less than 10% of the total fuel is burned).

Focusing on the analysis of the pre-chamber combustion, Fig. 8 shows the energy balance performed in this region during the ejection process. In this figure, the absolute value of energy are depicted in the left graph and the relative contribution respect to the total energy available at the start of the ejection are plotted on the right side.

The full length of each bar in the left graph represents the energy available at the beginning of the ejection process. Within these bars, the yellow share corresponds to the energy lost during cold/non-reacting ejection, when pressure is increasing inside the pre-chamber but the flame front has not reached the holes yet. The orange share is the energy lost by heat transfer through the pre-chamber walls. Finally, the blue share is the remaining energy available for ejection (EAE), this is the effective energy used for igniting the main chamber.

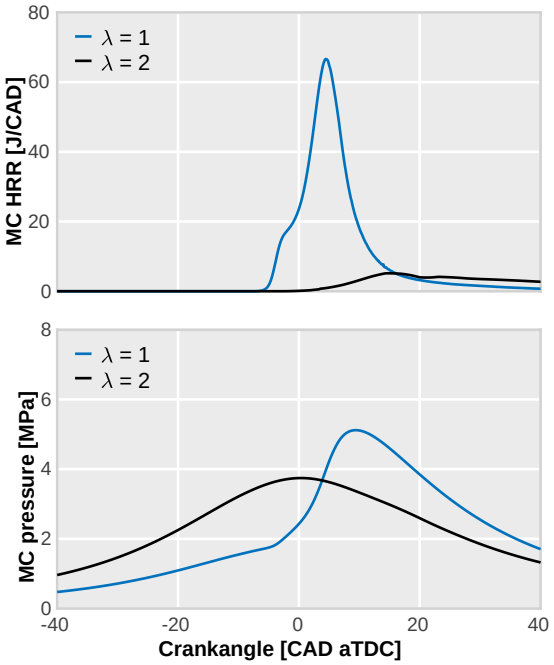

Figure 7: *Comparison among $\lambda = 1$ and $\lambda = 2$ simulations. The HRR and pressure traces in the main chamber are shown.*

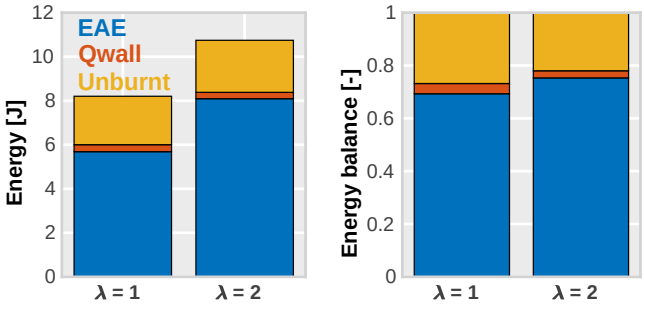

Figure 8: *Energy balance inside the pre-chamber during the ejection process. Simulations at $\lambda = 1$ and $\lambda = 2$ are compared.*

Comparing the energy balance for both simulations ($\lambda = 1$ and $\lambda = 2$), it is clearly seen that the available energy for the $\lambda = 2$ case is higher. This is mainly due to the pressure increase necessary to achieve the desired operating condition (note that the fuel amount was kept constant in both conditions). Although the amount of fuel in the cylinder is the same as the stoichiometric case, the higher pressure ratio upstream and downstream the pre-chamber holes results in a larger amount of energy within the pre-chamber at the spark timing due to the additional mixture mass included into. This also contributes to enhance the EAE ratio from 69% in the stoichiometric case to 75% in the ultra-lean case.

Moreover, the amount of heat transferred towards the walls scarcely changes, being below 5% of the total energy available in both cases. This is direct consequence of the small volume of the pre-chamber and due to the fact that the ejection process takes place during a short period of time. Thus, the effective energy gains achievable by minimizing the heat transfer loss in the pre-chamber are basically negligible. This statement will be confirmed further on this paper through additional simulations.

Despite the additional EAE indirectly achieved at $\lambda = 2$ conditions, jets features are still insufficient to assure a reasonable combustion rate in the main chamber. This suggests that the EAE should be further increased to compensate the combustion rate reduction observed at ultra-lean conditions. Therefore, further parameters, specifically related to the combustion process itself, should be analysed in detail to completely understand the concept operation.

The laminar flame speed evaluated in the flame region, the HRR and the relative pressure (Δp) defined as the pressure difference between the pre-chamber and the main chamber are included in Fig. 9. Examination of these parameters sheds some light on the root of the main chamber combustion issues when operating at $\lambda = 2$. For instance, the laminar flame speed values depicted in the top graph are four times lower at ultra-lean conditions when compared with stoichiometric conditions, being probably the main cause of the refereed combustion issues. Moreover, the HRR profiles, plotted in the middle graph, show that the maximum energy release due to combustion in the pre-chamber is reduced by almost half and the combustion duration is extended as a consequence of the lower laminar flame speeds. This subsequently affects to the maximum pressure difference among both chambers as can be seen in the bottom graph, compromising the ejection process and the ignition of the main chamber.

It is important to point out that the second peak in the HRR profile of the $\lambda = 1$ case is due to the back-flow from the main chamber to the pre-chamber once combustion in the main chamber has started. Therefore, only the first peak of the HRR will be taken into account when analysing these profiles, since the second is no longer representative of the jet ejection process.

Analyzing more in depth the combustion process, Fig 10 shows the evolution of the flame as combustion progresses in both the pre-chamber and the main chamber. In this figure, the flame tracking is made by colouring the local energy release, which corresponds to the source term of the energy equation, in two different cut planes. An axial cut plane parallel to the pre-chamber axis is considered for the visualization of pre-chamber ignition and combustion whereas the main chamber combustion is shown on a horizontal cut plane orthogonal to the cylinder axis and located 3 mm away form the pre-chamber bottom. In addition, in these latter snapshots the limits of the jets are highlighted as a contour line to easily identify where combustion occurs.

Inspection of the first sequence (top), shows a conventional premixed flame ignition and propagation inside the pre-chamber at $\lambda = 1$ and $\lambda = 2$ conditions. In both cases, a clear flame structure is observed after the ignition onset that sweeps the pre-chamber from the position of the spark plug to the bottom of the pre-chamber, where the holes are. There

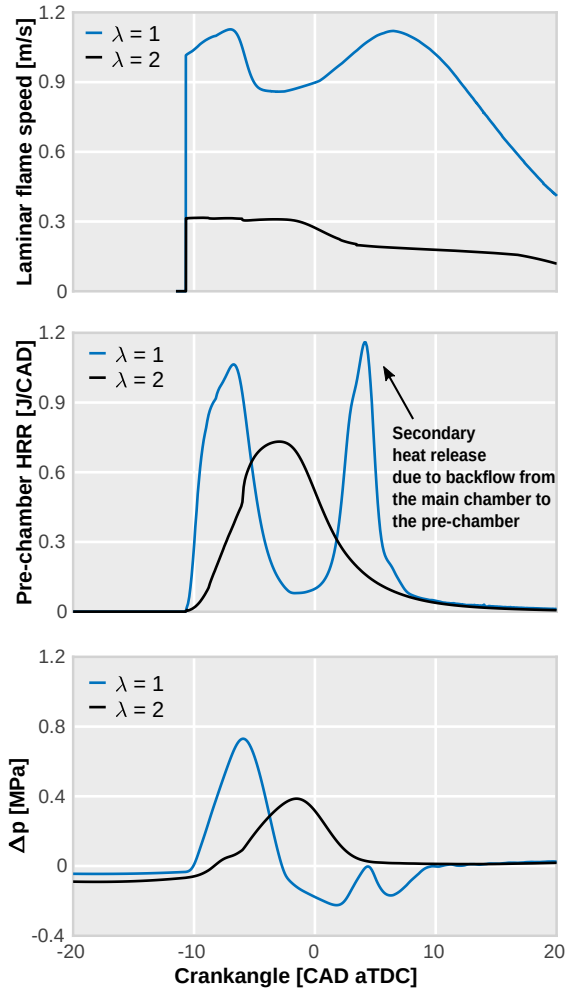

Figure 9: *Comparison among $\lambda = 1$ and $\lambda = 2$ simulations. The laminar flame speed evaluated in the flame region, HRR trace in the pre-chamber and pressure difference (Δp) profiles are shown.*

are two main differences between the two simulated conditions. Probably the most evident the different time scales observed among them. While the flame completely sweeps the pre-chamber in approximately 3 CAD in $\lambda = 1$, it needs almost 7 CAD when operating at $\lambda = 2$. This behaviour is directly related to the loss of laminar flame speed already discussed.

Once the pressure of the pre-chamber exceeds the pressure of the main chamber, the hot gases are ejected towards the main chamber. This forces the onset of combustion at multiple locations, as shown in the second sequence (bottom). In both cases, the ignition occurs inside the jets whereas the whole entrained fuel mass is consumed. However, only in the $\lambda = 1$ case the flame is able to progress outside the jets when the ejection finishes (around -3.0 CAD aTDC when the pressure difference among both chambers equilibrates). Conversely, thermochemical and turbulence properties downstream the jet bounds compromise the flame propagation in the $\lambda = 2$ case, leading to the flame extinction and releasing a minor part of the fuel energy available. This behaviour is better observed in the bottom graphs of the figure, where the amount of energy released inside and outside the jets are plotted for each case. It can be seen for the $\lambda = 1$ case that only a small part of the heat release process occurs inside the jets, as the flame quickly reaches the jet limits and thermodynamic conditions outside these boundaries are favourable for flame propagation. On the other hand, for the $\lambda = 2$ case it is clearly observed that practically the whole energy is released inside the jet bounds.

From this analysis, two limiting factors have been identified when operating at ultra-lean conditions. The first one is related to the low values of laminar flame speed during the combustion inside the pre-chamber. This fact worsens the flame structure and propagation velocity, compromising the pre-chamber pressurization and subsequently the ejection process. This effect can be clearly observed in the Borghi-Peters diagram presented in Fig. 11. In this figure, the evolution of the combustion regime as the pre-chamber combustion progresses is plotted for the $\lambda = 1$ case and the $\lambda = 2$ cases. The flame features move towards the *thickened flame* regime in which some eddies can penetrate into the diffusive layer of the flame structure, enlarging the flame thickness and compromising the flame stability.

The second constraint is also associated to the same root cause, but in the case of the main chamber, thermodynamic conditions inside the jets help to overcome the decrease in flame propagation speed associated to the increase in λ. Nonetheless, since the jets fail to entrain the whole mass of the main chamber, only a partial combustion can be achieved, as outside the jets the flame propagation speed is significantly lower than that of $\lambda = 1$. In the simulation of ultra-lean conditions the combustion efficiency does not reach 10%, revealing the low performance of the jets that are not able to sweep the entire combustion chamber. Therefore, the question that arises from this study is if it is possible to burn the available fuel in a reasonable time frame by improving the jets performance (at least equating them to those of the $\lambda = 1$ case), thereby overcoming the flame front propagation issues.

Based on this idea, a sensitivity analysis of air/fuel thermochemical properties was performed with the 1D laminar flame speed code. Fig. 12 shows the dependency of the laminar flame speed for blends of air and iso-octane to the temperature, pressure, relative air-to-fuel ratio and composition. The simulated conditions were conscientiously selected from the previous CFD simulations for being enough representative of the engine operation. It can be seen that the optimal value for this parameter when the air/fuel ratio is swept, corresponds to a slightly rich mixture of $\lambda = 0.95$. From this point, the flame speed decreases progressively with the air-to-fuel ratio up to three times lower value at $\lambda = 2$. The pressure dependency is characterized by an exponentially decreasing curve, reducing the flame velocity when increasing the pressure from 0.1 to 1.5 MPa and then remaining more or less constant from thereon. Conversely, the dependency of the temperature is defined by an exponentially increasing

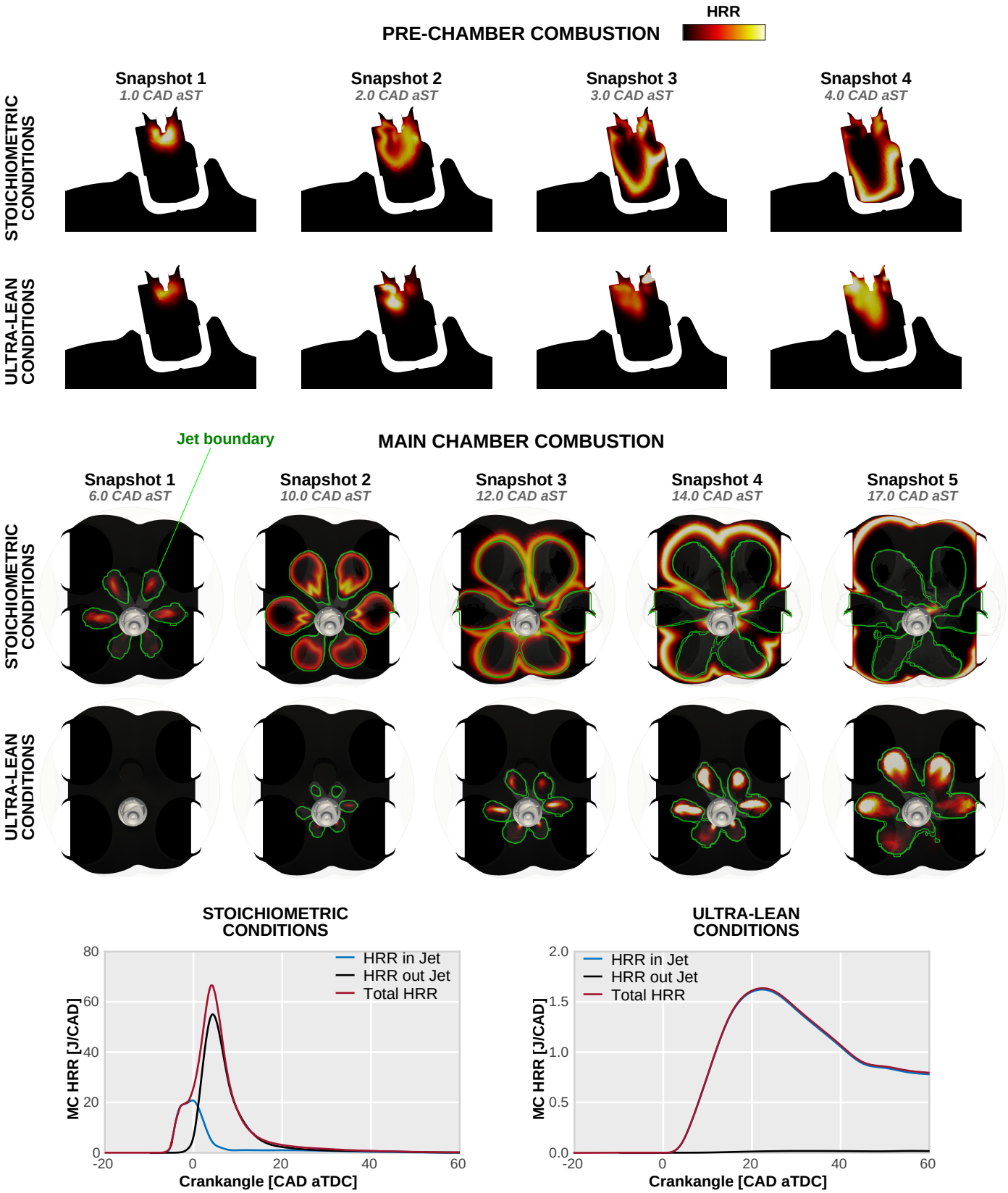

Figure 10: *Visualization of the ignition sequence at stoichiometric and ultra-lean conditions. The local energy release is used to track the position of the flame at a given snapshot whereas the limits of the jets are determined whit the help of a dynamic tracer. The HRR scale for ultra-lean conditions is 40 times lower than stoichiometric conditions for visualization purposes. The numeric values and evolution of the HRR profiles inside/outside the jets for both conditions are plotted in the bottom graphs.*

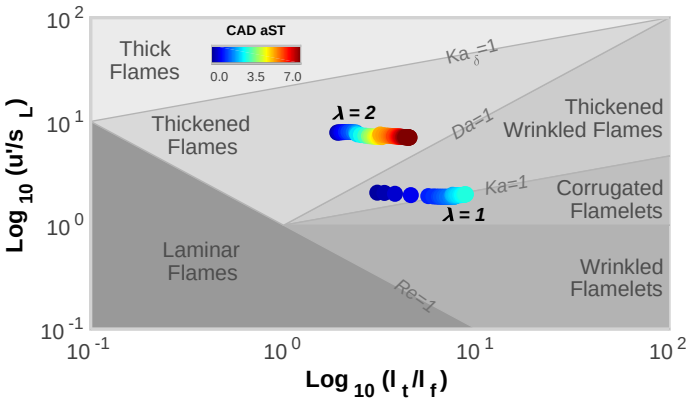

Figure 11: *Evolution of the flame regime as the pre-chamber combustion progresses.*

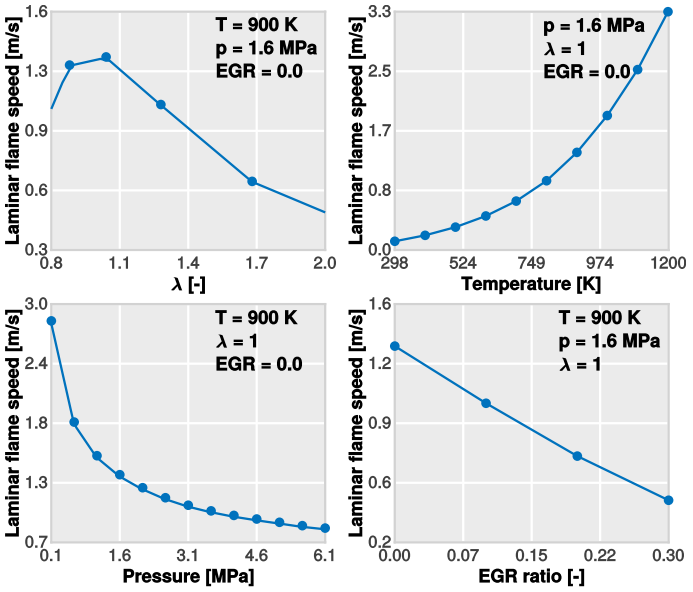

Figure 12: *Sensitivity study of air/iso-octane mixtures. Laminar flame speed is numerically estimated for a wide range of temperature, pressure and air-residuals dilution.*

curve that grows sharply when moving from 750K to 1200K. Lastly, the dilution with EGR also decreases the laminar flame speed. In this case, it is interesting to note that the laminar flame velocity drop observed when increasing the EGR level up to 30% is very similar to that shown when increasing the air dilution from $\lambda = 1$ to $\lambda = 2$, thus showing more sensitivity to dilution with residual gases than with air. This trend was also confirmed by Benajes et al. [42] using equivalent engine experiments.

The only thermochemical property of the flow that contribute to rise the laminar flame speed is therefore the temperature since the in-cylinder pressure is fixed by both the intake pressure and engine compression ratio and the mixture dilution goes against the laminar flame speed. Thus, increasing the flow temperature should compensate the loss of combustion performance observed when operating at ultra-lean conditions. In order to estimate the temperature in-

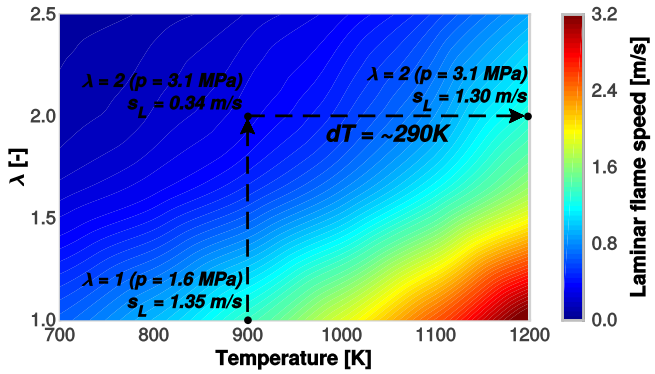

Figure 13: *Estimation of the flow temperature increase for recovering stoichiometric laminar flame speed values.*

crease necessary to recover the laminar flame speed values observed at stoichiometric conditions, further 1D simulations were performed. These results are included in Fig. 13 in which the evolution of the laminar flame speed is plotted against the relative air-to-fuel ratio and the flow temperature. The level of EGR was fixed to zero as in the engine simulations whereas the pressure conditions were obtained from the registered values inside the pre-chamber just before the spark timing. In these maps, the trajectory to go from $\lambda = 1$ to $\lambda = 2$ is included. The first point of this path starts at 900K of temperature, 1.6 MPa of pressure, $\lambda = 1$ and 1.35 m/s of laminar flame speed, coinciding with the conditions within the pre-chamber at the stoichiometric engine simulation. Then, the laminar flame speed shifts to a less favourable region in the map (0.34 m/s) when λ is increased to 2. In this second point, the temperature is 900K (intake temperature remained constant among both engine tests) and the pressure increased up to 3.1 MPa (intake pressure raised to keep the same amount of fuel as in the stoichiometric test while shifting to $\lambda = 2$). Thus, an increase of 290K is required to recover the $\lambda = 1$ values of laminar flame speed.

After the estimation of the target flow temperature, a set of simulations were performed to achieve suitable ultra-lean combustion considering several realistic situations. The first option to be evaluated was to directly increase the intake flow temperature until reaching the desired value inside the pre-chamber. In the same way, the intake pressure was increased to keep the same amount of fuel as in the previous engine tests while maintaining $\lambda = 2$ conditions. Results of this study in terms of in-cylinder pressure and HRR are shown in Fig. 14. As expected the increase in temperature promotes uncontrolled auto-ignition in both the pre-chamber and main chamber, producing extremely high HRR peaks and pressure gradients (knocking combustion). A visualization of this phenomenon in the pre-chamber is included in the top-right corner of this figure. As it can be seen, a hot spot located at the bottom of the pre-chamber appears downstream

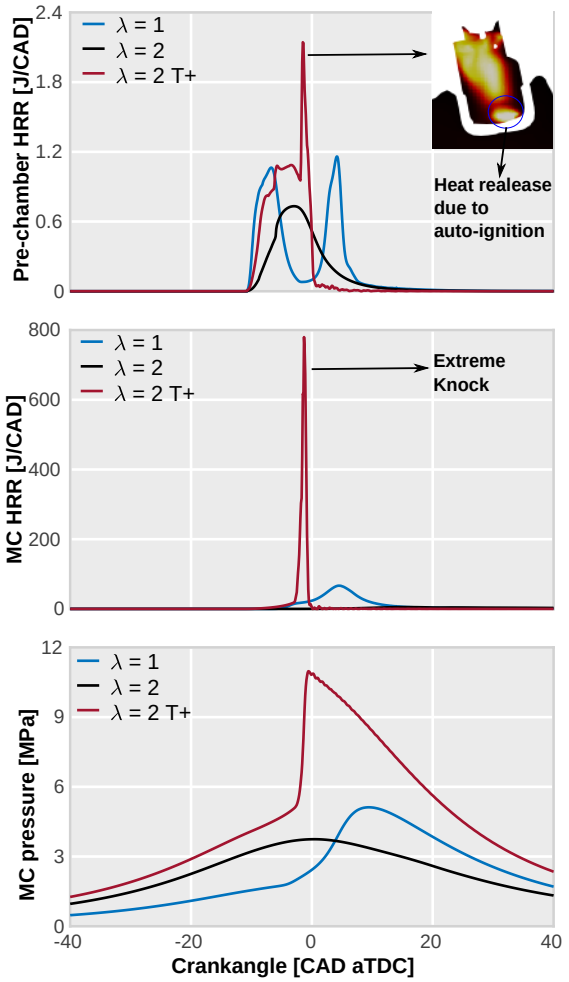

Figure 14: *Results of increasing the flow temperature at $\lambda = 2$ conditions. The HRR profiles in the pre-chamber and main chamber and the in-cylinder pressure are included.*

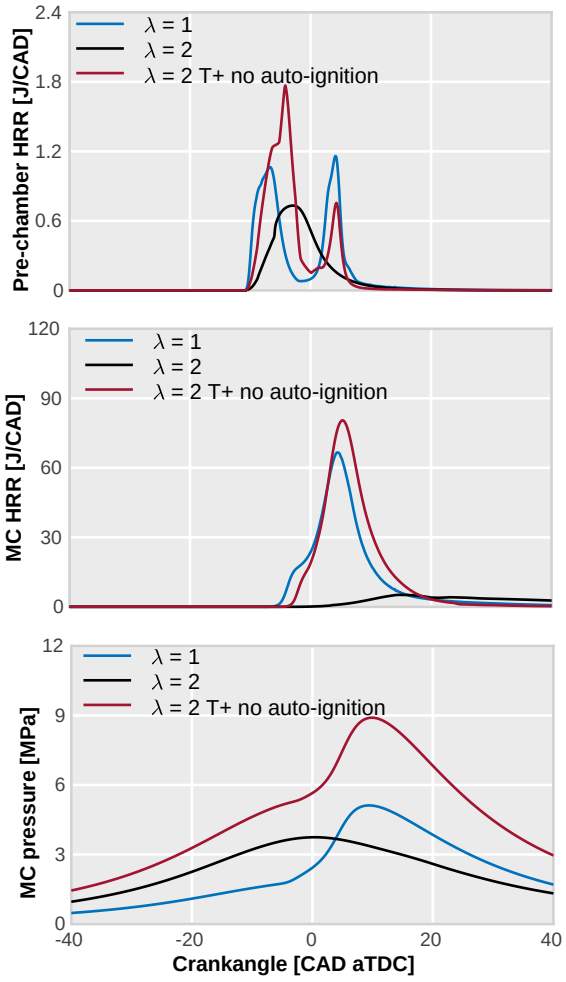

Figure 15: *Effects of increasing the flow temperature at $\lambda = 2$ conditions with the auto-ignition model deactivated. The HRR profiles in the pre-chamber and main chamber and the in-cylinder pressure are included.*

the flame propagation path, rapidly consuming the remaining unburned charge. This phenomenon is also replicated in the main chamber.

Thus, the implementation of this strategy in the current engine architecture and with the current fuel is clearly impossible as the risk of engine failure is very high. However, it might be interesting to evaluate this strategy using a similar fuel with higher RON to avoid abnormal combustion. In order to check if, with these kind of fuels, it made sense to implement this strategy, an additional simulation was performed.

Therefore, the auto-ignition model was deactivated from the CFD simulation while keeping the laminar flame speed features of the gasoline fuel. This simulation allows to evaluate, at least in a qualitative way, the proposed strategy to recover the combustion rate when knock is not a stringent constraint (i.e. when using high resistant knock fuels such as Compressed Natural Gas).

Inspecting the comparison shown in Fig. 15, significant improvements can be found if the flow temperature is increased. The combustion rate in the main chamber is recovered and the burning rate is similar to stoichiometric conditions in both the pre-chamber and the main chamber. The energy balance shown in Fig. 16 exhibits an increase in the EAE if it is compared even with the reference $\lambda = 2$. Again, this is explained by the intake pressure increase needed to maintain the amount of fuel among all tests and conditions. In this case, the effect of air dilution and flow temperature should be compensated with a large pressure increase. This additional energy available for igniting the main chamber contributes positively to recover the combustion rate of the main chamber by enhancing the turbulence conditions. Note that the maximum HRR in the main chamber (Fig. 15) is higher for the $\lambda = 2$ T+ case than for the stoichiometric case.

Moreover, analysing Fig. 17, these improvements are not only related to the increase in laminar flame speed. Although the increment of the flow temperature (∼250K) is not as high

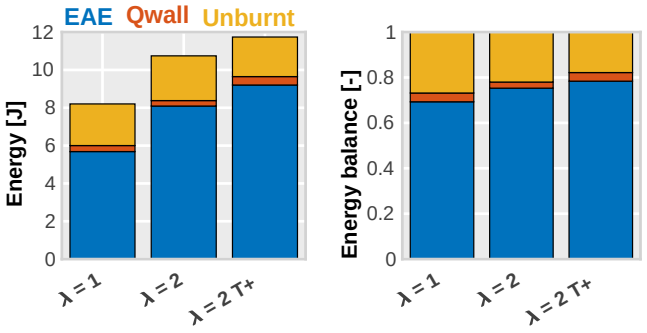

Figure 16: *Energy balance inside the pre-chamber during the ejection process, comparing the simulations at $\lambda = 1$, $\lambda = 2$ and $\lambda = 2$ with increased flow temperature (with the auto-ignition model deactivated).*

as the value estimated in the preliminary evaluation study (∼290K, see Fig. 13), the laminar flame speed is still doubled during the pre-chamber combustion, but never reaching the stoichiometric values. However, the increase in pressure to achieve ultra-lean conditions has 2 more effects that physically favours the combustion process. First, as explained in the previous graph, it produces a greater mass flow exchange between both chambers, resulting in a 12% increment in the fuel mass available in the pre-chamber at the start of ejection, and second, the Turbulent Kinetic Energy (TKE) in the pre-chamber, depicted in the bottom graph, is three times greater than the $\lambda = 1$ case, which helps to increase the propagation speed of the flame.

It is the combination of these effects that allows to achieve the higher combustion rates shown in Fig. 15. Finally, the Borghi-Peters diagram shown in Fig. 18 evidences how the flame structure of the ultra-lean case is able to shift to a more favourable regime with the temperature increase, allowing a faster and more stable combustion process inside the pre-chamber.

Following the idea of increasing the temperature, the next step was to try to recover the combustion profile by acting only on the pre-chamber. So, instead of directly increasing the intake flow temperature, an attempt to only increase the temperature inside the pre-chamber was performed. From a more realistic point of view, this target can be achieved by two different approaches: minimizing heat losses in the pre-chamber by adding a ceramic or other low thermal conductivity material or even heating up the pre-chamber walls (using a pre-chamber wall heating system or a pre-heating glow plug typically used in Diesel engines).

In order to evaluate the effect of using a ceramic coating, an additional simulation considering adiabatic inner pre-chamber walls was carried out, to estimate the maximum gain in terms of temperature with a complete and perfect insulation. For this simulation the heat transfer was completely neglected by using adiabatic boundary conditions for the pre-chamber walls.

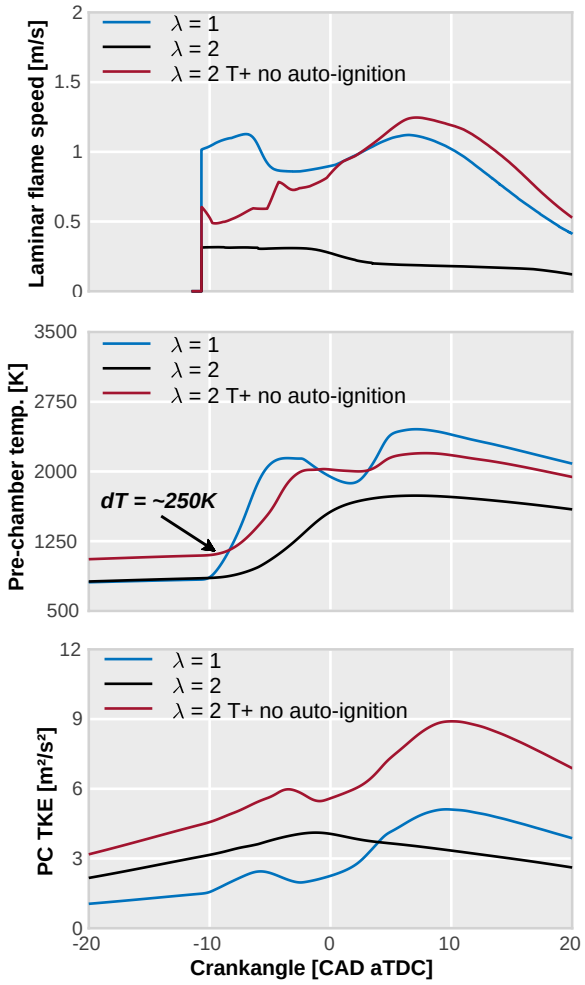

Figure 17: *Causes of the improved combustion features by increasing the mean flow temperature. A comparison of the laminar flame speed, pre-chamber flow temperature and pre-chamber TKE is shown.*

As expected from the previous energy analysis, Fig. 19 shows a negligible energy gain when using an adiabatic pre-chamber, reaching only a 2.8% of improvement in EAE. Although not shown in the graph, the temperature increase inside the pre-chamber is around 10K at the spark-timing. Therefore, as it can be seen in Fig. 20, only a slight increment of 0.02 m/s in the laminar flame speed is achieved.

Finally, a step forward was taken by artificially including a heating surface inside the pre-chamber in order to heat up the flow temperature. The temperature of the inner pre-chamber wall boundary was increased to 1000K and 1400K, being typical values of maximum pre-heating glow plug temperatures (ceramic and non-ceramic, respectively). Since flow conditions are not directly altered, the flow pressure and temperature at the start of the simulation were kept constant as in the reference $\lambda = 2$ case.

The energy balance for these cases is shown in Fig. 21 and an interesting pattern is observed. As this strategy solely affects the transient evolution of temperature inside the pre-

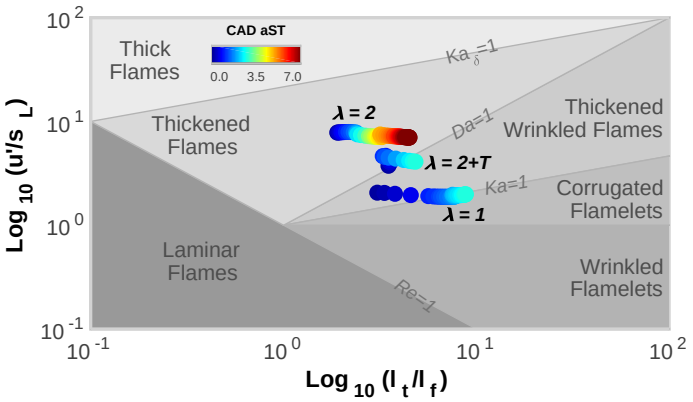

Figure 18: *Evolution of the flame regime as the pre-chamber combustion progresses. The $\lambda = 1$, $\lambda = 2$ and $\lambda = 2$ with increased temperature cases are compared.*

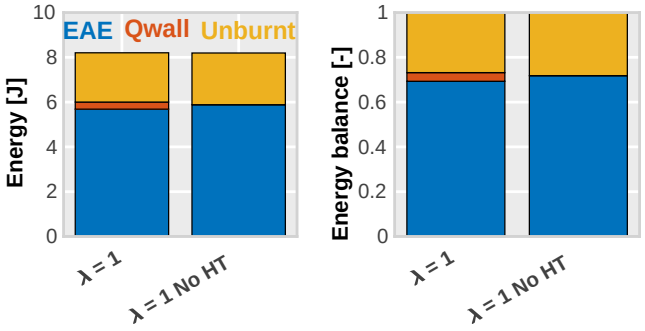

Figure 19: *Energy balance inside the pre-chamber during the ejection process, comparing the simulations for $\lambda = 1$ and $\lambda = 1$ with a perfect insulated pre-chamber.*

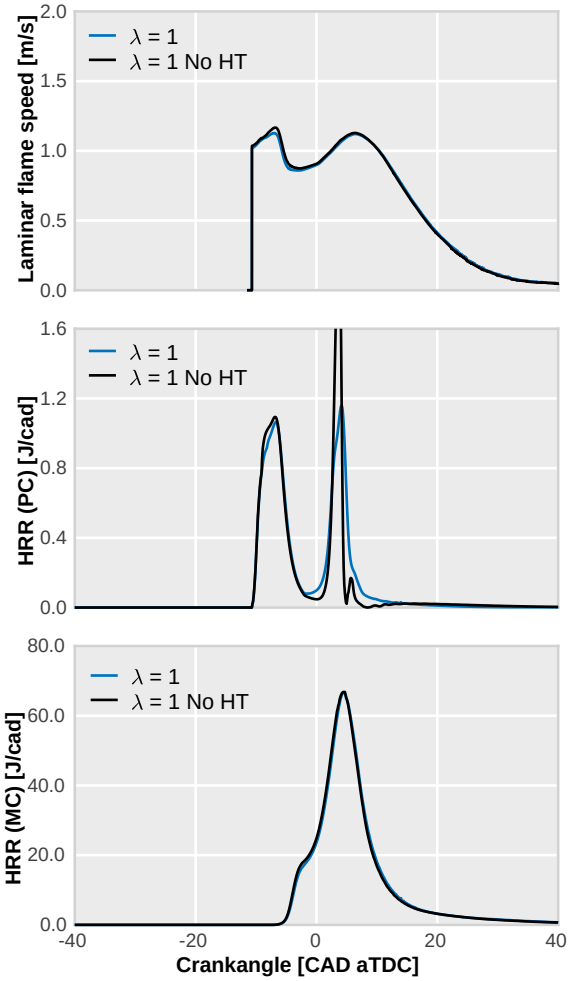

Figure 20: *Effects of applying a complete thermal insulation to the pre-chamber walls. The laminar flame speed and HRR profiles in the pre-chamber and main chamber are included.*

chamber, the mass flow exchange between both chambers is being compromised as the pre-chamber flow increases its temperature due to reverse heat transfer (from the walls to the flow). Thus, the total energy available tends to decrease as the flow temperature rises, decreasing the density inside the pre-chamber while hindering the re-chamber filling. Nonetheless, the effective EAE scarcely changes in all these cases due to a significant reduction of ejected unburnt mass. The case with the wall temperature increased to 1400K achieves almost 90% of EAE ratio. This is mainly due to the higher burning rate achieved inside the pre-chamber that allows the flame to reach earlier the pre-chamber holes.

As it can be seen in Fig. 22 the laminar flame speed is initially recovered if the temperature of the wall is increased to 1400K, reaching similar values to those achieved at $\lambda = 1$ in the early stage of the pre-chamber combustion. Although some knock is seen in the pre-chamber HRR profile, it is sufficiently small to neglect the detrimental effect it could cause to the inner pre-chamber walls. However, the values of laminar flame speed rapidly decrease as combustion penetrates into the main chamber, resulting in the HRR profile also included in the figure. While the energy release in the pre-chamber tends to match with the $\lambda = 1$ simulation, it scarcely increases respect to the $\lambda = 2$ case in the main chamber. Hence, the significant improvements in terms of jet ejection parameters are still not sufficient to adequately burn the lean charge of the main chamber.

5. Summary and conclusions

A computational methodology for evaluating the passive pre-chamber ignition concept at ultra-lean conditions for gasoline SI engines is presented in this paper. It has been proven how this methodology is an adequate procedure for analysing both the scavenge and combustion processes of passive pre-chambers. The CFD model has been successfully validated with the experimental data for both conventional SI and TJI concepts at stoichiometric conditions. An energy balance of the passive pre-chamber was performed, providing insight about the characteristics of the concept in terms of inert ejection, heat transfer through the pre-chamber walls and the effective energy available for the main chamber ignition. Moreover, the results are relevant to understand the ignition system limitations when operating at ultra-lean conditions.

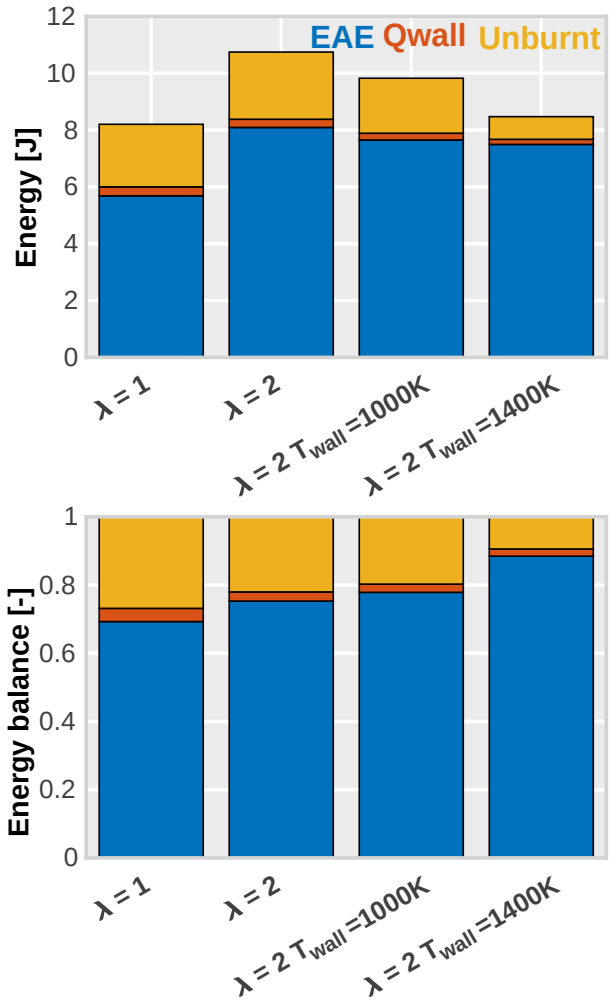

Figure 21: *Energy balance inside the pre-chamber during the ejection process, comparing the simulations for $\lambda = 1$, $\lambda = 2$ and $\lambda = 2$ with increased pre-chamber wall temperature.*

The analysis of the pre-chamber scavenge allowed to determine some design guidelines for a suitable pre-chamber configuration. The main findings extracted from the study of the pre-chamber scavenge are:

- The pre-chamber scavenge is mainly controlled by the force that the piston makes on the gas during the compression stroke and barely changes with the geometrical parameters as long as the pre-chamber A/V ratio is maintained within an appropriate range. Combinations of big volumes and small orifices worsens the scavenging process.
- There is a given amount of residual gases, directly related with the compression ratio, that cannot be evacuated from the pre-chamber, making the concept very sensible to EGR dilution due to the inherent residual gases present in this region. Furthermore, advancing the spark timing sharply increases residual gases at the beginning of the pre-chamber combustion.

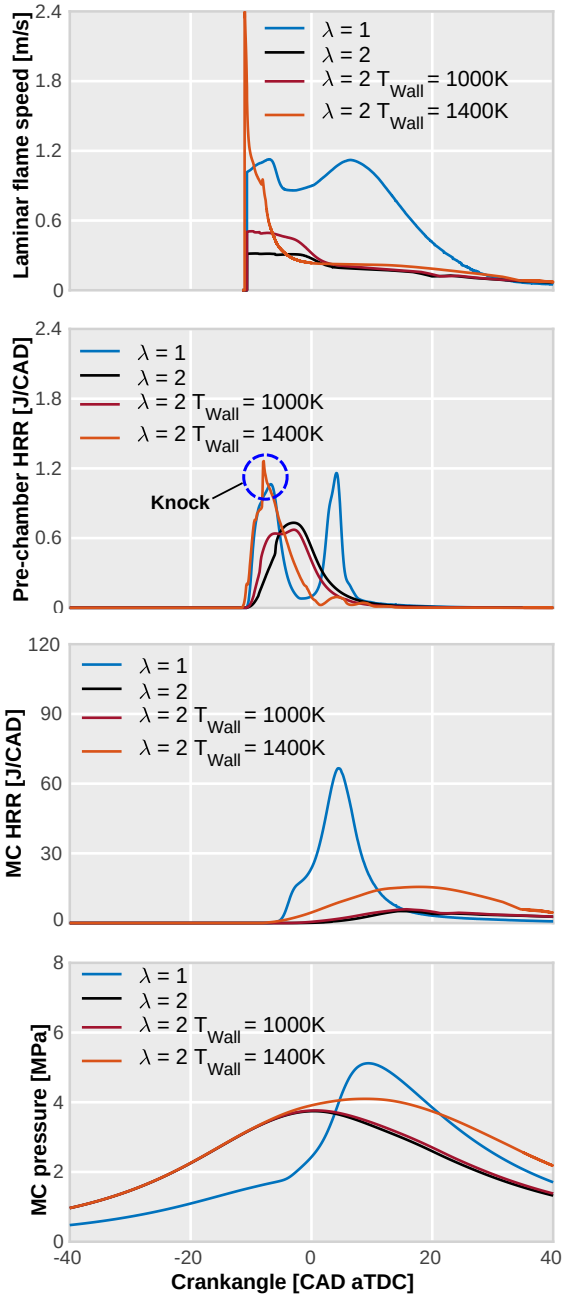

Figure 22: *Effects of increasing the pre-chamber inner wall temperature at $\lambda = 2$ conditions. The laminar flame speed, HRR profiles in the pre-chamber and main chamber and the in-cylinder pressure are included.*

The results operating in ultra-lean conditions showed that:

- The contribution of heat transfer losses to the energy balance of the pre-chamber is basically negligible (less than 5% of the total energy available), due to the small volume of the pre-chamber and short duration of the ejection process.

- A suitable jet ejection process is not only related to the effective amount of energy available for ejection but also on the velocity on which that energy is consumed, which mostly depends on thermo-chemical conditions inside the pre-chamber.
- A significant reduction in the laminar flame speed at ultra-lean conditions has been confirmed, that compromises the combustion process in two different ways. Firstly, the low combustion rates shown inside the pre-chamber compromises its pressurization and therefore, the quality of the ejected jets. Secondly, the flame is not able to progress properly outside the jets and only the jets entrained charge is successfully consumed.
- Increasing the mean flow temperature helps to extend the dilution range above the values of conventional SI engines. However, this must be combined with high knock resistant fuels to avoid engine integrity issues during operation.
- The impact of the pre-chamber insulation in the flow temperature has been evaluated. Minimizing the heat losses through the pre-chamber walls by using ceramic materials only provides a marginal improvement in laminar flame speeds and subsequently in HRR profiles.
- The effects of heating the pre-chamber flow by external energy sources has also been evaluated. Although this strategy increases the efficiency of the pre-chamber (the energy available for ejection is maintained while the total energy decreases) and the combustion rate inside this region, the properties of the ejected jets are not sufficient to ensure a suitable combustion in the main chamber as the flame propagation outside the jet bounds are really compromised.

Further studies will be carried out to analyze other fundamental aspects of the passive pre-chamber ignition concept and to evaluate new strategies for extending the air dilution limit of this ignition strategy. Analyzing more in depth the turbulence properties and jet characteristics is expected to help improve the understanding of the governing mechanisms of this ignition concept.

Acknowledgements

The authors want to express their gratitude to CONVERGENT SCIENCE Inc. and Convergent Science GmbH for their kind support for the 0D, 1D and CFD calculations with the CONVERGE software.

The work has been partially supported by the Spanish Ministerio de Economía y Competitividad through grant number TRA2017-89139-C2-1-R.

J. Gomez-Soriano is partially supported through the Programa de Apoyo para la Investigación y Desarrollo (PAID) of Universitat Politècnica de València [grant number FPI-S2-2018-17367].

[1] J. Conti, P. Holtberg, J. Diefenderfer, A. LaRose, J. T. Turnure, L. Westfall, International energy outlook 2016 with projections to 2040, Tech. rep., USDOE Energy Information Administration (EIA), Washington, DC (United States ... (2016).

[2] S. C. Davis, S. W. Diegel, R. G. Boundy, et al., Transportation energy data book, Tech. rep., Oak Ridge National Laboratory (2009).

[3] A. Vressner, P. Gabrielsson, I. Gekas, E. Senar-Serra, Meeting the euro vi nox emission legislation using a euro iv base engine and a scr/asc/doc/dpf configuration in the world harmonized transient cycle, Tech. rep., SAE Technical Paper (2010).

[4] J. Wang, H. Chen, Z. Hu, M. Yao, Y. Li, A review on the pd-based three-way catalyst, Catalysis Reviews 57 (1) (2015) 79–144.

[5] R. M. Heck, R. J. Farrauto, Automobile exhaust catalysts, Applied Catalysis A: General 221 (1-2) (2001) 443–457.

[6] W. P. Attard, S. Konidaris, F. Hamori, E. Toulson, H. C. Watson, Compression ratio effects on performance, efficiency, emissions and combustion in a carbureted and pfi small engine, Tech. rep., SAE Technical Paper (2007).

[7] M. B. Celik, Experimental determination of suitable ethanol–gasoline blend rate at high compression ratio for gasoline engine, Applied Thermal Engineering 28 (5-6) (2008) 396–404.

[8] A. J. Torregrosa, A. Broatch, J. García-Tíscar, J. Gomez-Soriano, Modal decomposition of the unsteady flow field in compression-ignited combustion chambers, Combustion and Flame 188 (2018) 469–482. doi:10.1016/j.combustflame.2017.10.007.

[9] J. Pan, H. Wei, G. Shu, M. Pan, D. Feng, N. Li, Les analysis for auto-ignition induced abnormal combustion based on a downsized si engine, Applied Energy 191 (2017) 183–192. doi:10.1016/j.apenergy.2017.01.044.

[10] T. Tsurushima, E. Kunishima, Y. Asaumi, Y. Aoyagi, Y. Enomoto, The Effect of Knock on Heat Loss in Homogeneous Charge Compression Ignition Engines, SAE 2002 World Congress & Exhibitiondoi:10.4271/2002-01-0108.

[11] A. Misdariis, O. Vermorel, T. Poinsot, LES of knocking in engines using dual heat transfer and two-step reduced schemes, Combustion and Flame 162 (11) (2015) 4304–4312. doi:10.1016/j.combustflame.2015.07.023.

[12] R. R. Maly, R. Klein, N. Peters, G. Konig, Theoretical and Experimental Investigation of Knock Induced Surface Destruction, International Congress & Expositiondoi:10.4271/900025.

[13] M. Kowada, I. Azumagakito, T. Nagai, N. Iwai, R. Hiraoka, Study of Knocking Damage Indexing Based on Optical Measurement, SAE 2015 World Congress & Exhibitiondoi:10.4271/2015-01-0762.

[14] A. Al-Sarkhi, J. Jaber, S. Probert, Efficiency of a miller engine, Applied Energy 83 (4) (2006) 343–351.

[15] J. Zhao, Research and application of over-expansion cycle (atkinson and miller) engines–a review, Applied Energy 185 (2017) 300–319.

[16] A. Broatch, P. Olmeda, X. Margot, J. Gómez-Soriano, Numerical simulations for evaluating the impact of advanced insulation coatings on h2 additivated gasoline lean combustion in a turbocharged spark-ignited engine, Applied Thermal Engineering 148 (2019) 674–683.

[17] G. J. Germane, C. G. Wood, C. C. Hess, Lean combustion in spark-ignited internal combustion engines-a review, Tech. rep., SAE Technical Paper (1983).

[18] E. J. Tully, J. B. Heywood, Lean-burn characteristics of a gasoline engine enriched with hydrogen from a plasmatron fuel reformer, SAE transactions (2003) 851–864.

[19] W. P. Attard, H. Blaxill, A lean burn gasoline fueled pre-chamber jet ignition combustion system achieving high efficiency and low nox at part load, Tech. rep., SAE Technical Paper (2012).

[20] D. Sarkar, Thermal power plant: design and operation, Elsevier, 2015.

[21] S. Tsuboi, S. Miyokawa, M. Matsuda, T. Yokomori, N. Iida, Influence of spark discharge characteristics on ignition and combustion process and the lean operation limit in a spark ignition engine, Applied Energy 250 (2019) 617–632.

[22] T. Aoyama, Y. Hattori, J. Mizuta, Y. Sato, An experimental study on premixed-charge compression ignition gasoline engine, Tech. rep., SAE Technical paper (1996).

[23] A. Broatch, R. Novella, J. García-Tíscar, J. Gomez-Soriano, On the shift of acoustic characteristics of compression-ignited engines when operating with gasoline partially premixed combustion, Applied Thermal Engineering 146 (2019) 223–231. doi:10.1016/j.applthermaleng.2018.09.089.

[24] Z. Wang, J.-X. Wang, S.-J. Shuai, Q.-J. Ma, Effects of spark ignition and stratified charge on gasoline hcci combustion with direct injection, Tech. rep., SAE Technical Paper (2005).

[25] S. Biswas, L. Qiao, Ignition of ultra-lean premixed hydrogen/air by an impinging hot jet, Applied energy 228 (2018) 954–964.

[26] S. Biswas, L. Qiao, Ignition of ultra-lean premixed h2/air using multiple hot turbulent jets generated by pre-chamber combustion, Applied Thermal Engineering 132 (2018) 102–114.

[27] S. Heyne, M. Meier, B. Imbert, D. Favrat, Experimental investigation of prechamber autoignition in a natural gas engine for cogeneration, Fuel 88 (3) (2009) 547 – 552. doi:https://doi.org/10.1016/j.fuel.2008.09.032.
URL http://www.sciencedirect.com/science/article/pii/S0016236108003712

[28] Q. Malé, G. Staffelbach, O. Vermorel, A. Misdariis, F. Ravet, T. Poinsot, Large eddy simulation of pre-chamber ignition in an internal combustion engine, Flow, Turbulence and Combustion (2019) 1–19.

[29] G. Xu, Y. M. Wright, M. Schiliro, K. Boulouchos, Characterization of combustion in a gas engine ignited using a small unscavenged pre-chamber, International Journal of Engine Research (2018) 1468087418798918.

[30] E. Toulson, H. J. Schock, W. P. Attard, A review of pre-chamber initiated jet ignition combustion systems, Tech. rep., SAE Technical Paper (2010).

[31] W. P. Attard, E. Toulson, A. Huisjen, X. Chen, G. Zhu, H. Schock, Spark ignition and pre-chamber turbulent jet ignition combustion visualization, Tech. rep., SAE Technical Paper (2012).

[32] C. E. C. Alvarez, G. E. Couto, V. R. Roso, A. B. Thiriet, R. M. Valle, A review of prechamber ignition systems as lean combustion technology for si engines, Applied Thermal Engineering 128 (2018) 107–120.

[33] W. P. Attard, P. Parsons, A normally aspirated spark initiated combustion system capable of high load, high efficiency and near zero nox emissions in a modern vehicle powertrain, SAE International Journal of Engines 3 (2) (2010) 269–287.

[34] W. P. Attard, H. Blaxill, E. K. Anderson, P. Litke, Knock limit extension with a gasoline fueled pre-chamber jet igniter in a modern vehicle powertrain, SAE International Journal of Engines 5 (3) (2012) 1201–1215.

[35] M. Kettner, M. Rothe, A. Velji, U. Spicher, D. Kuhnert, R. Latsch, A new flame jet concept to improve the inflammation of lean burn mixtures in si engines, SAE transactions (2005) 1549–1557.

[36] J. R. C. Gomes, R. M. Valle, F. J. P. Pujatti, J. P. Pereira, Torch ignition system analysis in an spark ignition engine, Tech. rep., SAE Technical Paper (2005).

[37] E. Toulson, H. C. Watson, W. P. Attard, Modeling alternative prechamber fuels in jet assisted ignition of gasoline and lpg, Tech. rep., SAE Technical Paper (2009).

[38] Y. Zeldovich, D. Frank-Kamenetskii, P. Sadovnikov, Oxidation of nitrogen in combustion, Publishing House of the Acad of Sciences of USSR, 1947.

[39] G. Gentz, M. Gholamisheeri, E. Toulson, A study of a turbulent jet ignition system fueled with iso-octane: Pressure trace analysis and combustion visualization, Applied energy 189 (2017) 385–394.

[40] U. Spicher, T. Heidenreich, Stratified-charge combustion in direct injection gasoline engines, in: Advanced Direct Injection Combustion Engine Technologies and Development, Elsevier, 2010, pp. 20–44.

[41] J. Benajes, R. Novella, J. Gomez-Soriano, P. Martinez-Hernandiz, C. Libert, M. Dabiri, Performance of the passive pre-chamber ignition concept in a spark-ignition engine for passenger car applications, in: SIA Power Train & Electronics, SIA Power Train & Electronics, Paris, France, 2019.

[42] J. Benajes, R. Novella, J. Gomez-Soriano, P. Martinez-Hernandiz, C. Libert, M. Dabiri, Evaluation of the passive pre-chamber ignition concept for future high compression ratio turbocharged spark-ignition engines, Applied Energy 248 (2019) 576–588.

[43] F. Payri, S. Molina, J. Martín, O. Armas, Influence of measurement errors and estimated parameters on combustion diagnosis, Applied Thermal Engineering 26 (2) (2006) 226 – 236. doi:https://doi.org/10.1016/j.applthermaleng.2005.05.006.
URL http://www.sciencedirect.com/science/article/pii/S1359431105001560

[44] M. Lapuerta, O. Armas, J. Hernández, Diagnosis of di diesel combustion from in-cylinder pressure signal by estimation of mean thermodynamic properties of the gas, Applied Thermal Engineering 19 (5) (1999) 513 – 529. doi:https://doi.org/10.1016/S1359-4311(98)00075-1.
URL http://www.sciencedirect.com/science/article/pii/S1359431198000751

[45] C. Guardiola, J. López, J. Martín, D. García-Sarmiento, Semiempirical in-cylinder pressure based model for nox prediction oriented to control applications, Applied Thermal Engineering 31 (16) (2011) 3275–3286.

[46] CONVERGENT SCIENCE Inc., CONVERGE 2.4 Theory Manual (2018).

[47] V. Yakhot, S. A. Orszag, Renormalization group analysis of turbulence. i. basic theory, Journal of scientific computing 1 (1) (1986) 3–51.

[48] R. Cant, Sb pope, turbulent flows, cambridge university press, cambridge, uk, Combustion and Flame 125 (2001) 1361–1362.

[49] C. Angelberger, T. Poinsot, B. Delhay, Improving near-wall combustion and wall heat transfer modeling in si engine computations, Tech. rep., SAE Technical Paper (1997).

[50] O. Redlich, J. N. Kwong, On the thermodynamics of solutions. v. an equation of state. fugacities of gaseous solutions., Chemical reviews 44 (1) (1949) 233–244.

[51] F. E. Marble, J. E. Broadwell, The coherent flame model for turbulent chemical reactions, Tech. rep., PURDUE UNIV LAFAYETTE IN PROJECT SQUIDHEADQUARTERS (1977).

[52] P. Boudier, S. Henriot, T. Poinsot, T. Baritaud, A model for turbulent flame ignition and propagation in spark ignition engines, in: Symposium (International) on Combustion, Vol. 24, Elsevier, 1992, pp. 503–510.

[53] O. Colin, A. Benkenida, C. Angelberger, 3d modeling of mixing, ignition and combustion phenomena in highly stratified gasoline engines, Oil & gas science and technology 58 (1) (2003) 47–62.

[54] O. Colin, A. Benkenida, The 3-zones extended coherent flame model (ecfm3z) for computing premixed/diffusion combustion, Oil & Gas Science and Technology 59 (6) (2004) 593–609.

[55] T. Poinsot, D. Veynante, Theoretical and numerical combustion, RT Edwards, Inc., 2005.

[56] O. Colin, K. Truffin, A spark ignition model for large eddy simulation based on an fsd transport equation (issim-les), Proceedings of the Combustion Institute 33 (2) (2011) 3097–3104.

[57] J. Duclos, O. Colin, (2-25) arc and kernel tracking ignition model for 3d spark-ignition engine calculations ((si-7) si engine combustion 7-modeling), in: The Proceedings of the International symposium on diagnostics and modeling of combustion in internal combustion engines 01.204, The Japan Society of Mechanical Engineers, 2001, p. 46.

[58] R. I. Issa, Solution of the implicitly discretised fluid flow equations by operator-splitting, Journal of computational physics 62 (1) (1986) 40–65.

[59] A. Torregrosa, P. Olmeda, B. Degraeuwe, M. Reyes, A concise wall temperature model for di diesel engines, Applied Thermal Engineering 26 (11-12) (2006) 1320–1327.

[60] Y.-D. Liu, M. Jia, M.-Z. Xie, B. Pang, Enhancement on a skeletal kinetic model for primary reference fuel oxidation by using a semidecoupling methodology, Energy & Fuels 26 (12) (2012) 7069–7083.

[61] H. Wang, M. Yao, R. D. Reitz, Development of a reduced primary reference fuel mechanism for internal combustion engine combustion simulations, Energy & Fuels 27 (12) (2013) 7843–7853.

[62] L. Cai, H. Pitsch, Optimized chemical mechanism for combustion of gasoline surrogate fuels, Combustion and flame 162 (5) (2015) 1623–1637.

[63] M. Mehl, W. J. Pitz, C. K. Westbrook, H. J. Curran, Kinetic modeling of gasoline surrogate components and mixtures under engine conditions, Proceedings of the Combustion Institute 33 (1) (2011) 193–200.

[64] K. Fieweger, R. Blumenthal, G. Adomeit, Self-ignition of si engine model fuels: a shock tube investigation at high pressure, Combustion and Flame 109 (4) (1997) 599–619.
[65] D. Davidson, B. Gauthier, R. Hanson, Shock tube ignition measurements of iso-octane/air and toluene/air at high pressures, Proceedings of the Combustion Institute 30 (1) (2005) 1175–1182.
[66] M. Metghalchi, J. C. Keck, Burning velocities of mixtures of air with methanol, isooctane, and indolene at high pressure and temperature, Combustion and flame 48 (1982) 191–210.
[67] Ö. L. Gülder, Correlations of laminar combustion data for alternative si engine fuels, Tech. rep., SAE Technical Paper (1984).
[68] J. Brakora, R. D. Reitz, A comprehensive combustion model for biodiesel-fueled engine simulations, Tech. rep., SAE Technical Paper (2013).
[69] S. Jerzembeck, N. Peters, P. Pepiot-Desjardins, H. Pitsch, Laminar burning velocities at high pressure for primary reference fuels and gasoline: Experimental and numerical investigation, Combustion and Flame 156 (2) (2009) 292–301.
[70] S. Heimel, R. C. Weast, Effect of initial mixture temperature on the burning velocity of benzene-air, n-heptane-air, and isooctane-air mixtures, in: Symposium (international) on combustion, Vol. 6, Elsevier, 1957, pp. 296–302.
[71] O. Vermorel, S. Richard, O. Colin, C. Angelberger, A. Benkenida, D. Veynante, Towards the understanding of cyclic variability in a spark ignited engine using multi-cycle LES, Combustion and Flame 156 (8) (2009) 1525–1541. doi:10.1016/j.combustflame.2009.04.007.
[72] M. Sens, E. Binder, P. Reinicke, M. Riess, et al., Pre-chamber ignition and promising complementary technologies, in: 27th Aachen Colloquium, Aachen, 2018.

List of Figures

1 Computational domain and mesh details for non-reacting and reacting simulations. 5
2 Auto-ignition delays validation for different iso-octane mechanisms at engine-like conditions. . 5
3 Laminar flame speed validation for different iso-octane mechanisms at engine-like conditions. 5
4 Experimental validation of the CFD model in terms of in-cylinder pressure and rate of heat release operating with conventional SI (top) and TJI (bottom) concepts. 6
5 Diagram of the methodology developed for the present research work. 7
6 Scavenge diagrams for the considered pre-chamber designs. The origin of the different flows are tracked by the defined tracers. 7
7 Comparison among $\lambda = 1$ and $\lambda = 2$ simulations. The HRR and pressure traces in the main chamber are shown. 9
8 Energy balance inside the pre-chamber during the ejection process. Simulations at $\lambda = 1$ and $\lambda = 2$ are compared. 9
9 Comparison among $\lambda = 1$ and $\lambda = 2$ simulations. The laminar flame speed evaluated in the flame region, HRR trace in the pre-chamber and pressure difference (Δp) profiles are shown. 10
10 Visualization of the ignition sequence at stoichiometric and ultra-lean conditions. The local energy release is used to track the position of the flame at a given snapshot whereas the limits of the jets are determined whit the help of a dynamic tracer. The HRR scale for ultra-lean conditions is 40 times lower than stoichiometric conditions for visualization purposes. The numeric values and evolution of the HRR profiles inside/outside the jets for both conditions are plotted in the bottom graphs. 11
11 Evolution of the flame regime as the pre-chamber combustion progresses. 12
12 Sensitivity study of air/iso-octane mixtures. Laminar flame speed is numerically estimated for a wide range of temperature, pressure and air-residuals dilution. 12
13 Estimation of the flow temperature increase for recovering stoichiometric laminar flame speed values. 12
14 Results of increasing the flow temperature at $\lambda = 2$ conditions. The HRR profiles in the pre-chamber and main chamber and the in-cylinder pressure are included. 13
15 Effects of increasing the flow temperature at $\lambda = 2$ conditions with the auto-ignition model deactivated. The HRR profiles in the pre-chamber and main chamber and the in-cylinder pressure are included. 13
16 Energy balance inside the pre-chamber during the ejection process, comparing the simulations at $\lambda = 1$, $\lambda = 2$ and $\lambda = 2$ with increased flow temperature (with the auto-ignition model deactivated). 14
17 Causes of the improved combustion features by increasing the mean flow temperature. A comparison of the laminar flame speed, pre-chamber flow temperature and pre-chamber TKE is shown. 14
18 Evolution of the flame regime as the pre-chamber combustion progresses. The $\lambda = 1$, $\lambda = 2$ and $\lambda = 2$ with increased temperature cases are compared. 15
19 Energy balance inside the pre-chamber during the ejection process, comparing the simulations for $\lambda = 1$ and $\lambda = 1$ with a perfect insulated pre-chamber. 15
20 Effects of applying a complete thermal insulation to the pre-chamber walls. The laminar flame speed and HRR profiles in the pre-chamber and main chamber are included. 15
21 Energy balance inside the pre-chamber during the ejection process, comparing the simulations for $\lambda = 1$, $\lambda = 2$ and $\lambda = 2$ with increased pre-chamber wall temperature. 16

22 Effects of increasing the pre-chamber inner wall temperature at $\lambda = 2$ conditions. The laminar flame speed, HRR profiles in the pre-chamber and main chamber and the in-cylinder pressure are included. 16

List of Tables

1 Main specifications of the engine. 3
2 Experimental baseline test conditions. 3
3 Pre-chamber designs and specifications. 8